Comparison of Ion and Neutron Irradiations to 3 dpa at 500°C in Ferritic-Martensitic Alloys

M.J. Swenson[1], J.P. Wharry[1]

[1] *Boise State University*
1910 University Dr., Boise, ID 83725
matthewswenson1@u.boisestate.edu

INTRODUCTION

The growing global demand for energy will increasingly call upon advanced nuclear fission reactors to supply safe and reliable electricity. The structural and fuel cladding components of these reactors will be subject to extreme conditions of irradiation damage up to several hundred displacements per atom (dpa) at temperatures as high as 700°C. Ferritic-martensitic (F-M) steels are leading candidates for these challenging conditions due to their strength and dimensional stability under irradiation.

In order to accelerate the process for evaluating F-M alloys, charged particles are increasingly being used to emulate neutron irradiations. Charged particle irradiations allow the possibility of conducting irradiation experiments within a shorter time period (i.e. at a rate up to 4 orders of magnitude faster) and with minimal radioactivation of the material, enabling lower cost and faster turnaround of post irradiation examination and analysis. However, the irradiation dose rate, damage cascade morphologies, and irradiation damage depth profiles all differ widely between protons, heavier ions, and neutrons. Currently, there is limited understanding of the significance of these physical differences and how they manifest in the irradiated microstructure and mechanical properties of F-M steels.

The objective of this study is to evaluate charged particles as a surrogate for neutron irradiations in F-M alloys by assessing common irradiation conditions using Fe^{++} ions, protons, and neutrons. Keeping the temperature and dose consistent enables isolation of the effects of each irradiating particle and their respective dose rates and cascade morphologies.

EXPERIMENTS

Material and Irradiations

Experiments focused on the commercial F-M alloys HCM12A (~11%Cr) and HT9 (~12%Cr). Alloy compositions are provided in Table I. Three sets of specimens were prepared from the same heat of each alloy: one set for 2 MeV proton irradiation (dose rate ~10^{-5} dpa/sec), another set for 5 MeV self-ion (Fe^{++} ion) irradiation (~10^{-4} dpa/sec), and another set for neutron irradiation (~10^{-7} dpa/sec). All of these irradiations were carried out to 3 dpa at 500°C to enable a direct comparison of irradiation effects across different dose rates and irradiating particles, but otherwise consistent conditions.

Table I. Compositions (wt%) of HCM12A, HT9 (bal. Fe)

Element	HCM12A	HT9
Cr	10.5	12.1
C	0.09	0.171
Si	0.30	0.41
V	-	0.34
Mn	0.52	0.61
Ni	1.04	0.59
Cu	1.5	0.025
Mo	0.26	0.97
W	1.43	0.58

HCM12A also includes trace amounts of N, P, Nb, Ta
HT9 also includes trace amounts of N, O, Al, P, S, Ti, Co

Metallographic sample preparation was carried out on all specimens prior to irradiation. Both charged particle irradiations were conducted using a 1.7 MV General Ionex Tandetron Accelerator at the Michigan Ion Beam Laboratory. The accelerator beam line was maintained at pressures below 10^{-7} torr and the irradiation temperature was maintained at 500 ± 10°C. Displacement damage was calculated with the Stopping and Range of Ions in Matter (SRIM) software in "Quick Calculation (K-P)" mode for the Fe^{++} ion irradiation and in "Detailed Calculation" mode for the proton irradiation. The damage profile for both irradiations in "Quick Calculation (K-P)" mode are illustrated in Fig. 1, with a flat neutron damage profile of arbitrary magnitude for comparison of damage profile shapes. Microstructural measurements were conducted at depths of 1-7 μm in the proton irradiated specimens, and 400-600 nm in the self-ion irradiated specimens in order to avoid any surface effects and the steep irradiation dose gradient at the damage peak.

Neutron irradiation specimens were similarly prepared, then irradiated in a fast neutron spectrum in the Advanced Test Reactor at the Idaho National Laboratory. The irradiation temperature of 500°C was determined with SiC electrical resistivity samples placed in experiment capsules; thermal models correlated the SiC resistivity measurements.

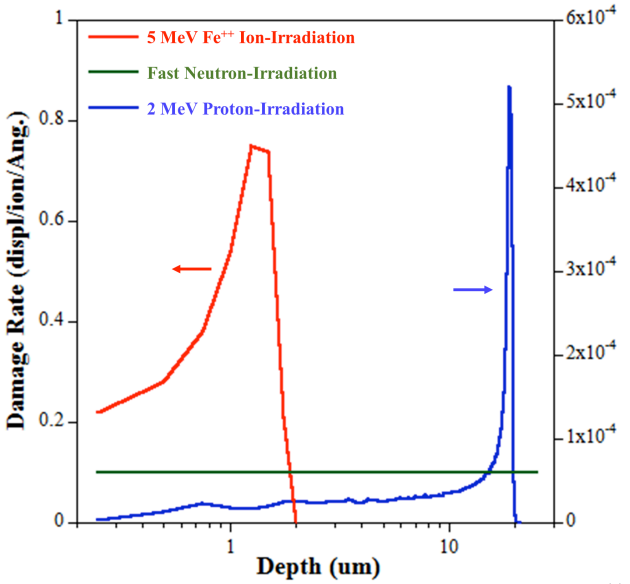

Fig. 1. SRIM simulated damage profiles for 5.0 MeV Fe^{++} ions and 2.0 MeV protons incident on HCM12A or HT9, along with a flat neutron damage profile of arbitrary magnitude for reference.

Transmission electron microscopy

Sample lamellae were prepared for each irradiation condition with an FEI Quanta 3D FEG focused ion beam (FIB) at the Center for Advanced Energy Studies (CAES). Each specimen was cut and lifted perpendicular to the bulk surface. The microstructures were characterized using an FEI Tecnai TF30-FEG scanning transmission electron microscope (STEM) at CAES with emphasis on measuring size and number density of grains, dislocations, carbide precipitates, voids (if present), and dislocation loops. Grains, carbides, dislocations, and voids were imaged in bright field mode, with the through-focus technique used for identification of any voids. Dislocation loops were imaged in STEM mode following a procedure outlined by Parish et al. [1], in which small collection (β) and convergence (α) angles are applied to create a STEM bright field image. Finally, the specimen thickness was measured with electron energy loss spectroscopy (EELS).

Atom probe tomography

Sample needles were prepared from each irradiation condition using FIB, and each needle was analyzed with a Cameca LEAP 4000X HR at CAES. Each LEAP data set was reconstructed with the Integrated Visualization and Analysis Software (IVAS) Version 3.6.2 using the voltage history during the LEAP analysis. Each tip rendering was visually inspected to ensure the tip shape was consistent with the SEM image prior to analysis.

Elements were identified using their mass-to-charge ratio, with peaks based on overall isotope abundance given the known composition of the material. Cluster analysis was performed on each tip using the maximum separation method [2], with the parameter d_{max} and N_{min} selected to minimize any spurious detection of clusters. Using the IVAS cluster analysis output data, which includes a radius of gyration (R_g) for each cluster, the Guinier diameter (D_G) for each cluster was determined using:

$$D_G = 2\sqrt{\frac{5}{3}}R_g \qquad (1)$$

The overall cluster number density was calculated as:

$$N_{nc} = \frac{\sum N_C}{\sum V_T} \qquad (2)$$

where ΣN_C is the total number of clusters identified in all tips from a given specimen and ΣV_T is the total analyzed volume in all tips from that specimen.

RESULTS

Transmission electron microscopy

For both HCM12A and HT9, the measurements of grains and carbides were statistically invariant between each irradiation condition. In the HCM12A specimens, average grain and carbide sizes ranged 0.61-0.66 μm and 0.07-0.11 μm, respectively. Carbide number densities ranged 0.35-0.97 x 10^{20} m^{-3}, and dislocation line density varied over 12.1-13.6 x 10^{14} m^{-2}. In the HT9 specimens, average grain and carbide sizes ranged 0.30-0.41 μm and 0.06-0.07 μm, respectively. Carbide number densities ranged 0.62-0.71 x 10^{20} m^{-3}, and dislocation line density varied over 13.6-14.1 x 10^{14} m^{-2}. Based on these relatively narrow bands of size and density measurements, there is no evidence to suggest that carbides and dislocation lines have dramatically evolved in response to any of the irradiation conditions.

Dislocation loop sizes and number densities were consistent across all irradiation conditions and alloys (Fig. 2). In the HCM12A specimens, average loop sizes ranged 7.5-7.7 nm with densities ranging 2.2-4.4 x 10^{21} m^{-3}. A slightly lower density in the self-ion irradiated HCM12A is likely due to a thicker TEM sample that made identification of loops more difficult. In the HT9 specimens, average loops sizes ranged 7.5-7.6 nm with densities ranging 2.0-2.4 x 10^{21} m^{-3}. Dislocation loop orientation maps generated by Yao et al. [3] were used to confirm that the loops commonly resided on the {111} or {001} habit planes. Voids were not observed in any of the irradiated HCM12A or HT9 specimens.

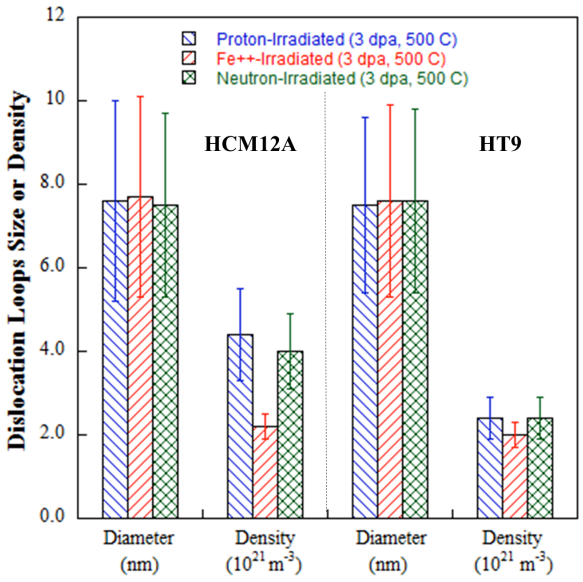

Fig. 2. Dislocation loop size and density measurements in irradiated specimens of HCM12A and HT9.

Atom probe tomography

The 3D reconstructions of the specimens from each alloy specimen enabled comparison of irradiation-induced clustering. In the irradiated HCM12A specimens, clusters rich in Si, Mn, Ni and P were observed adjacent to Cu-rich clusters (Fig. 3a). Average diameter of these clusters were markedly different at 9.22±3.57 nm, 4.65±1.28 nm, and 3.59±1.44 nm for the proton-, Fe-, and neutron-irradiated specimens, respectively. Similarly, measured number densities varied at $25x10^{21}$ m^{-3}, $87x10^{21}$ m^{-3}, and $580x10^{21}$ m^{-3}, respectively. Meanwhile, only the neutron-irradiated HCM12A specimen displayed Cr-rich clustering with an average diameter of 2.50±0.55 nm and density of $628x10^{21}$ m^{-3}, while the other HCM12A samples did not exhibit Cr-rich clusters (Fig. 3b).

For the irradiated HT9 specimens, clusters rich in Si, Mn, Ni and P were observed in only the proton- and neutron-irradiated specimens (Fig. 3c). Average diameter of these clusters was 6.38±4.22 nm and 5.22±4.27 nm for the proton- and neutron-irradiated specimens, respectively. The Fe-irradiated HT9 specimen did not demonstrate clustering of these elements, but did display segregation of these elements to grain and carbide boundaries. Once again, only the neutron-irradiated HT9 condition displayed Cr-rich clustering with an average diameter of 2.70±0.59 nm and density of $1572x10^{21}$ m^{-3}, while the other HT9 conditions did not exhibit Cr-rich clusters (Fig. 3d).

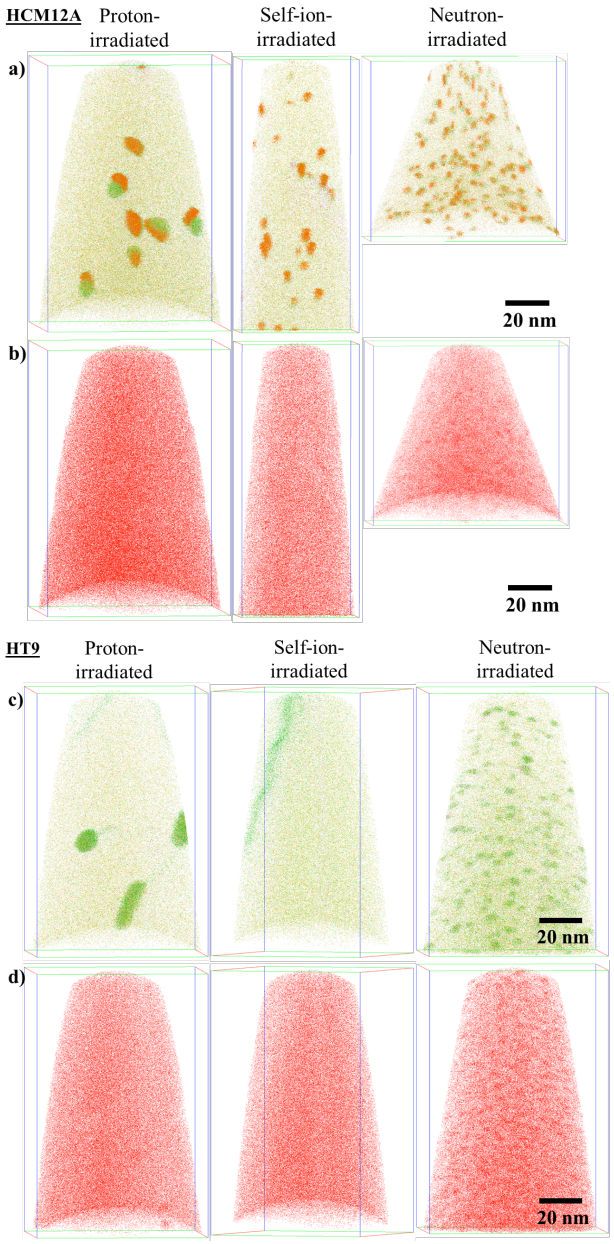

Fig. 3. Atom probe maps of HCM12A filtered to show elements: a) Si, Mn, Ni, P, Cu and b) Cr, and of HT9 filtered to show elements: c) Si, Mn, Ni, P, Cu and d) Cr.

DISCUSSION

The size and number density of microstructural features such as grains, carbides, dislocations and dislocation loops are generally consistent after each irradiation for both alloys. It follows that both proton and self-ion irradiation can likely reproduce the microstructure evolution of neutron irradiation for these features without an irradiation temperature shift.

Conversely, nanocluster nucleation and evolution for Si-Mn-Ni-P, Cu-rich, and Cr-rich clusters was markedly different between proton, Fe, and neutron irradiation. It has been hypothesized [4-6] that cluster evolution may be driven by two competing influences: (1) ballistic disordering (or dissolution) from irradiation damage cascades, and (2) thermal diffusion leading to coarsening. The ballistic effects are potentially dependent upon the cascade morphology of different irradiation particles. Proton irradiations generate multiple small-volume cascades in the target material, heavier ions create larger cascades, and neutrons create the largest cascades [7]. On the other hand, the coarsening rate of clusters is primarily dependent on diffusion, which may also be irradiation influenced as increases in dose rate lead to higher vacancy concentrations and accelerated diffusion rates for solute atoms. Furthermore, Mansur [8] theorized a temperature increase is necessary in order to produce consistent microstructure when the irradiation dose rate increases.

In HCM12A, proton irradiation produces the coarsest Si-Mn-Ni-P and Cu-rich clusters, while neutron irradiation produces the finest clusters. This trend is counter to the Mansur theory and suggests that the irradiation damage cascade morphology may play a more dominant role in the cluster evolution. Larger-volume neutron irradiation cascades may promote disordering and re-dissolution of clusters that are attempting to nucleate and ripen. However, since the HT9 self-ion irradiated sample did not display clustering of any elements, irradiation dose rate may also have an effect. Irradiation-induced clustering is likely a complex process influenced by both cascade morphology and dose rate.

Neutrons are the only irradiating particle that has produced Cr-rich clusters in both HCM12A and HT9. These alloys contain 10.5 and 12.1 wt% Cr, respectively, which is above the ~9% solubility limit of Cr in α-Fe. In these materials, then, if given enough energy and time, Cr will partially precipitate out of solution. For each of the irradiations conducted in this study, the temperature was kept consistent at 500°C. Therefore, the thermal diffusion rates of Cr would have been consistent across all experiments. Approximate irradiation times were 4 hours, 3.5 days and ~1 year for the self-ion, proton, and neutron irradiations, respectively. Thus, Cr clustering only in the neutron-irradiated specimens may be due to thermal aging at 500°C over ~1 year, rather than due to irradiation.

CONCLUSIONS

Specimens of HCM12A and HT9 were irradiated separately with protons, self-ions, and neutrons to a common dose of 3 dpa at 500°C. The microstructure of each specimen was characterized with TEM and LEAP and compared to evaluate proton and self-ion irradiation as a surrogate for neutron irradiation at these conditions.

- Proton, self-ion, and neutron irradiations produced consistent sizes and number densities of grains, carbides, dislocation lines, and dislocation loops. Voids were absent in all conditions. The charged particle irradiations have successfully reproduced the neutron irradiation results for these microstructural features without a temperature shift.
- Nanocluster evolution of Si-Mn-Ni-P and Cu-rich clusters was markedly different for each irradiating particle type. Some cluster morphology trends could be explained by differences in cascade volume for differing irradiating species. But dose rate likely also influences cluster evolution.
- Cr-rich nanoclusters nucleated only in the neutron-irradiated HCM12A and HT9. This is likely due to thermal aging at 500°C over a longer experimental time, as compared to the proton and self-ion irradiations.

REFERENCES

1. C.M. PARISH, "Application of STEM characterization for investigating radiation effects in BCC Fe-based alloys," *J. Mater. Res.*, **30** (2015).
2. J.M. HYDE, "A sensitivity analysis of the maximum separation method for the characterisation of solute clusters," *Ultramicroscopy*, **111**, 440-447 (2011).
3. B. YAO, D. J. EDWARDS, and R. J. KURTZ, "TEM characterization of dislocation loops in irradiated bcc Fe-based steels," *J. Nucl. Mater.*, **434**, 402-410 (2013).
4. G. MARTIN, "Phase stability under irradiation: Ballistic effects," *Phys. Rev.*, **30**, 1424-1436 (1984).
5. K.C. RUSSELL, "Phase instability under cascade damage irradiation," *J. Nucl. Mater.*, **206**, 129-138 (1993).
6. R.S. NELSON, "The stability of precipitates in an irradiation environment," *J. Nucl. Mater.*, **44**, 318-330 (1972).
7. G. S. WAS, *Fundamentals of Radiation Materials Science: Metals and Alloys*, p. 132, Springer (2007).
8. L.K. Mansur, "Theory of transitions in dose dependence of radiation effects in structure alloys," *J. Nucl. Mater.*, **206**, 306-323 (1993).

View publication stats